ORIGINAL RESEARCH (AR) DOI: 10.4274/jems.2024.97769

Journal of ETA Maritime Science 2024;12(1):74-82

Analysis of the Structure of Marine Propeller Blades for Ice Navigation

Aydın Bozkurt[1], Melek Ertogan[2]

[1]Istanbul Technical University, Graduate School of Science Engineering and Technology, Maritime Transportation Engineering Program, İstanbul, Türkiye
[2]Istanbul Technical University Faculty of Maritime, Department of Maritime Transportation and Management, İstanbul, Türkiye

Abstract

This study's analysis of the maritime propeller blade structure in ice navigation was motivated by an incident that caused the tip of a propeller blade to bend. The aim of this study was to demonstrate how the ice layer's confined space effect causes propeller blade tips to bend. Using computer-based software, a three-dimensional model of the propeller was created. The geometry of the three-dimensional propeller model was imported using the finite element approach into another piece of software. The propeller model and the environment were constructed after designing the ice environment. Using the computational fluid dynamics method, flux was calculated, and the composed pressure was derived. Following the specification of the alloy material for the propeller, the static structural module applied pressure values acquired to the propeller to measure the total deformation and stress. The data comparing the results of the simulation study are based on full-scale measurements. The maximum deformation in Ansys was 2.7-3.5 cm, whereas in the incident, it was 12 cm, which can be explained by persistent pressure or repeated initial movement steps. Considering these findings, the reason for blade tip bend, preventive measures, and recommendations have been proposed.

Keywords: Marine propeller, Ice navigation, Structure analysis, Computational fluid dynamics

1. Introduction

Shipping is a crucial component of global trade. Compared with other transportation modalities, large quantities of cargo can be transported over long distances for less money. As a result, ships travel on a variety of voyages, depending on cargo trade transactions, to practically every region of the world.

Diverse environments and locations expose ships to rare occurrences such as propeller blade deformation brought on by ice navigation. Analyses and evaluations of these unique occurrences must be disseminated throughout the maritime sector to prevent the recurrence of unfavorable effects. Propeller blade deformations, which can occur in both ducted and open-type propellers, are a significant issue for ice navigation. The cause of the blade deformations was found to be ice loads.

Hydrodynamic loads were studied on a high-density polyethylene propeller stopped by simulated ice in a cavitation tunnel. As they approached an obstacle larger than the propeller, they saw how erratic the thrust of a single blade might be, which led designers to account for impact and milling loads for strength and wear [1].

Experimental studies were conducted in a 200-mm cavitation tunnel with two open and two ducted propeller models. They studied the non-contact interaction between the propeller and ice that results in cavitation and obstruction. The ice block and propeller were subjected to a maximum pressure of 110 kPa, although this pressure was inadequate to cause the blade to deform. They claimed that cavitation was caused by decreased hydrodynamic loads, which were also ice milling loads for open-type propellers [2].

Address for Correspondence: Melek Ertogan, Istanbul Technical University Faculty of Maritime Department of Maritime Transportation and Management, İstanbul, Türkiye
E-mail: ertogan@itu.edu.tr
ORCID ID: orcid.org/0000-0002-9968-6254

Received: 13.08.2023
Last Revision Received: 05.11.2023
Accepted: 04.01.2024

To cite this article: A. Bozkurt., and M. Ertogan. "Analysis of the Structure of Marine Propeller Blades for Ice Navigation." *Journal of ETA Maritime Science*, vol. 12(1), pp. 74-82, 2024.

A process model was developed based on quasistatic contact and ignoring non-contact forces to penetrate an ice block by a propeller blade. Experimental study of leading edge machining of a large ice block. At full scale, it was claimed that sharp angles of attack caused the blades to bend backward, but the subject model did not fully consider these pressures [3].

The accumulation of total ice loads was studied, which includes separate hydrodynamic loads (cavitation-related proximity and blockage effects) and inseparable hydrodynamic loads (cavitation-related proximity and blockage effects). They used a 0.3-m diameter propeller and a "puller mode" podded propeller to analyze blade loads and cut depth. They calculated shaft thrust values for ice-related stresses using mounted dynamometers at varying cut depths [4].

Ice loads have been categorized into non-contact hydrodynamic and contact loads, focusing on open-water propulsion and ice blocks, highlighting their distinct differences [5].

The IACS Polar Class Rules (URI3) were used to optimize the strength and integrity of the polar class propellers. The study found that the out-of-plane bending moment is crucial for strength, considering spindle torque and the in-plane bending moment. The IACS found that Polar Classes 1 and 7 have equal strength requirements, and R Class propeller blades can save 1400 kg of material [6].

To simulate the propeller-ice contact at various advance coefficients, an ice block and a 2.8 m diameter, 120 rpm propeller were used. Using the ice class rule formula or the simulated model, they computed the blade ice load. The finite element method calculates propeller blade deformation based on the ice load. Advance coefficient increased blade distortion. A 6-m diameter, 0.7 EAR propeller was used to create a finite element method model for ice contact issues [7].

The transient propeller-ice block interaction in an ice milling scenario was modeled using peridynamics techniques. Their findings that the maximum force equals 9216.99 kN and the maximum moment equals 6007.40 kN m indicate that applied forces in the x-axis are the source of blade bending stress. For accurate numerical modeling, further investigation is advised [8].

The overlapping grids approach and CFD were used to predict the flow parameters and hydrodynamic performance of an ice-class propeller in the event of ice blockage. They used an ice block with dimensions of length: 200 mm, width: 200 mm, and height: 40 mm to test an ice-class 1 propeller with four blades and a diameter of 20 cm. The experimental test revealed a five percent difference in pressure, coefficients of thrust, and torque when the blade and ice block distance was less than 10% R. However, because of the rudder frame, keel, stern tube, and bottom of the aft hull body, finding an ice block smaller than 10% R is challenging [9].

CFD was utilized, and an overlap grid approach was used to analyze the exciting force generated by the propeller during ice block cutting. They found pressure variations in the P1 and P4 regions of a four-blade propeller and emphasized the three-stage decline caused by the interval between blade entry and ice block entry [10].

Five load scenarios were applied to the tip and furthest edges of a PC3 ice-class propeller, adhering to the IACS URI3 norm. They obtained stress and deformation values, developed a minimum safety factor of 1.5, and advised ice-class propellers to use this strength assessment approach during the design phase [11].

The hydrodynamic performance of a propeller was studied in a ship-model towing tank by adjusting the amount, size, and axial placement of synthetic ice. They used particle image velocimetry (PIV) to analyze the obstructed flow field of the propeller. This study discovered that thrust and efficiency are highly dependent on the model ice thickness. The torque and progress coefficients are negatively correlated with ice thickness. With constant advance coefficients, wider ice models have a greater impact on thrust and torque. Propeller efficiency is unaffected when the ice model width is greater than the propeller diamete. The PIV approach showed that the inflow velocity was lower than that in open water [12].

In ice-covered waters, the accelerating effect of the spinning propeller on brash ice is critical for a polar ship to break free of the ice. A new coupling model that uses computational fluid dynamics (CFD) and the discrete element method (DEM) is proposed to investigate brash ice loads and pressure fluctuations. The simulation results show that multiple peaks are caused by a low reversing speed, which accelerates and reduces ice loads. For optimal acceleration and pumping effects during moderate-speed reversals, fortifying the stern structure is advised [13].

Predicting self-propulsion performance is an important matter, and the brash ice channel is a crucial topic for polar ships. Using the CFD-DEM coupling approach, the propeller's hydrodynamic performance was simulated and the ice load was calculated. The simulation results accurately replicate the ship-ice and propeller-ice interaction processes, offering a technical tool for hull line building and navigation guidance in brash ice channels [14].

The Canadian Coast Guard investigated the connection between sea ice conditions and ice-induced propeller loads

in a study on ship operations in ice-covered seas. Using the Henry Larsen icebreaker as a case study, numerical analysis and experimental data were used to predict ice-induced impact loads on the propeller. The results showed considerable torque response values even in thin ice [15].

The safe and efficient operation of the Baltic Sea's winter navigation system is the aim of the Finnish-Swedish Ice Class Rules. In brash ice channels, vessel resistance is predicted using model-scale experiments. However, there are restrictions on the current norms. This study uses both full-scale and model-scale measurements to investigate the relationship between vessel resistance and brash ice qualities. For all hull forms, accurate modeling of the interaction between ice fragments enhances prediction quality [16].

The Baltic Sea is an area where ship performance is critical because different ice thicknesses have an impact on maneuverability and speed. Proposals have been made for numerical simulation techniques to improve accuracy and analyze complex operations. This research focuses on ship– ice interaction and proposed a framework for creating effective models. A prototype model is created, and its validity as a prototype is shown by contrasting simulation results with full-scale measurements [17].

This work analyzes numerical simulation approaches for ice tanks, dividing them into cohesive elements, discrete elements, lattice Boltzmann, smoothed particle hydrodynamics peridynamics and smoothed particle hydrodynamics. It assesses their effectiveness, precision, and usefulness in scenarios involving ship-ice contact. This study underlines the difficulties with current numerical techniques and stresses the significance of multidisciplinary applications in fluid-structure interactions [18].

Nearly all research concentrated on the contact load of ice, which was characterized as ice milling, impact, or contact of ice masses, and attempted to explain propeller blade deformation using various techniques, including ice tanks and cavitation tunnels. This study aims to demonstrate that the limited space impact of the ice layer causes propeller blade tips to bend in addition to the contact stresses of ice assumptions. If the ice layer is sufficiently thick and the suction side is not broken during the first part of the power-driven motion of the vessel, the tips of the propeller blades are bent until the ice layer breaks. It creates the illusion of an impermeable wall.

1.1. Investigate Investigating Propeller Blade Bent Incident in Iced North China Sea

Ice milling and ice block impact create contact stresses on the blades, causing permanent bends. The incident lacks indications of an ice milling groove, and the thinnest areas of blade tips and edges should also be deformed or have an ice milling groove. The blades should show impact indicators while assessing the impact of ice chunks. However, the bulb of a ship penetrates the ice as it moves forward, causing the bow to chisel out a split-like channel. Because the ship is 230 m long, it is above the ice layer and ice blocks aft of the ship, and big chunks of ice float instead of being dragged below. It is impossible to conclude that ice block contact or ice milling recess are the main causes of blade deformations in ice navigation because ducted propellers can also fail because of blade deformation.

Ice loads are non-contact loads that are too close to ice blocks, causing obstruction and ice milling. Ice block collisions or milling are likely to happen when traveling quickly and there is less than ten percent of the propeller's radius between it and the ice block. The rudder frame and stern tube, keel, and rear bottom hull shape prevent approaches to ice blocks with a diameter equal to that of the propeller.

The goal of this study is to demonstrate how the restricted space effect of the ice layer causes propeller blade tips to bend. If the ice layer is sufficiently thick and the suction side is not broken during the first part of the power-driven motion of the vessel, the tips of the propeller blades are bent until the ice layer breaks. It creates the illusion of an impermeable wall. Examine the propeller blade tip bend based on an incidence and use the inductive method to make generalizations. Full-scale measurements served as the basis for the data used to compare the outcomes of the simulation study. By the time this study is complete, a new word for the thick ice layer's enclosed space effect has been added to the literature.

This study investigates a propeller blade tip bend on a 230 m long bulk carrier in Liaodong Bay, North China Sea, and Bayuquan Port in January 2013. The enclosed space effect of the thick ice layer can cause of blade deformations.

The inductive technique was used to investigate the incident-based propeller blade tip bend in a range of propeller designs, including fixed-pitch, right-handed, four-bladed, low-skewed copper alloy (Cu 3) propellers. Despite the possibility of modeling a large variety of habitats, the study only supported astern propeller motion in a limited subset of environments.

2. Technical Details and a Description of the Incident

2.1. Description of the Incident

In January 2013, a Panamax ship encountered ice cover in Liaodong Bay, North China, as shown in Figures 1 and 2. The master advised dropping the anchor and reporting the

suspension to the Bayuquan Port Authority. The ice covering was 20-25 cm deep. The port authority instructed the ship to move forward to the pilot station, but the sea surface remained covered in ice, as shown in Figure 3. Despite pulling four tugs, the vessel could not reach the wharf for four hours due to ice masses re-accumulating.

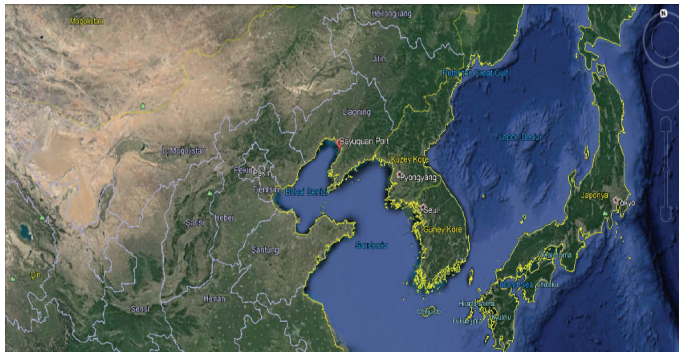

Figure 1. *Bayuquan Port, Liaodong Bay, North China*

Figure 2. *The roads around Bayuquan Port are covered in ice*

Figure 3. *Aft view of the Panamax ship at Bayuquan Port*

The ship, with a single main engine and fixed-pitch propeller, was moving around 25-30 m to the rear. With the help of a pilot and tugs, the ship was propelled backward. During the growth and freezing of the ice cover, the ship departed the quay with 2 pilots and 2 tugs. The master issued stern engine directives to leave the basin because of depth restrictions, but the engine's rpm did not rise quickly.

The ship's main engine is a four-bladed, right-handed engine with a fixed-pitch propeller. She was driven backward after loading the cargo. The ice covering broke, and the ship departed the wharf with 2 tugs and a pilot. The ship had a draft of 11.2 meters and approached from the basin's starboard side. Due to a basin depth restriction, the master left the berth using the astern engine directives. The ship was issued a dead slow forward command, but the engine's rpm did not rise quickly.

The ship's engine's rpm increased slowly and did not reach the desired level during its voyage. Initially, propeller fouling was suspected, but the outcome was negative. The ship was headed to Quanzhou, China, to load cargo. A diver survey of the propellers was conducted, but no irregularities were found. Singapore was the next stop for bunkering, and the shipyard service engineer was scheduled to visit. Upon landing, underwater inspection of the hull, propeller, and rudder was conducted, but no abnormal findings were found. The ship dropped anchor in Singapore to allow for more inspections. The diver requested a new survey of the propeller once more. Decided to measure the horizontal distance from the rudder frame to the propeller blades. Measurements showed that the tips of the propeller blades were bent. There were no signs of a likely significant impact.

2.2. Propeller Technical Information

The horizontal distances between each blade and rudder frame were measured by the divers in the Singapore AEBB anchoring area from four different locations, as shown in Figure 4. The horizontal distances between the rudder frame and the reference locations B, C, and D on each blade are the same. The horizontal length varies only at points A, 30 cm within the tip ends [19].

The horizontal distances of blades "1", "2", "3", and "4" from point A to the rudder frame were 272, 264, 265, and 260 cm, respectively.

According to the final diver report, all blade tips-aside from "1"-were bent between 7 and 12 cm toward the pressure side or the stern side of the ship.

Bulk Carrier, Panamax, 80,370 DWT, has one main engine and a fixed four-blade propeller. The main engine's maximum continuous output is 11,060 kW, and the maximum

revolution per minute is 127 rpm. The propeller's diameter, pitch at 0.7R, expanded area, skew are D:6.2 m, $P_{0.7}$:4.1362, A_e:15.548 m^2, and SK:23.856 deg, respectively. The other specifications are given in Table 1 [20].

3. Methodology of the Research

The ice propellers can be impacted by both non-contact (hydrodynamic) and contact (ice) loads. In this instance, the hydrodynamic tension on the blade serves as the non-contact load for propulsion in open water. The primary source of contact load is the ice load generated by the impact and ice milling processes. These non-contact and contact loads are very different from each other.

The literature employed a variety of methods to explain the deformation of propeller blades, including discrete, finite, and cohesive element methods, smoothed particle hydrodynamics, peridynamics lattice Boltzmann, and coupled models. The majority of these studies concentrated on the contact load of ice, which was defined as ice milling, impact, or contact of ice masses. Nevertheless, there was no indication of a likely significant impact on the propeller in the event involving the Panamax vessel, which lacks an ice-class propeller. Measurements showed that the tips of the propeller blades were bent. For comparison with the actual data, the widely used CFD method was chosen because the experienced scenario is not typical.

Three-dimensional propeller models were created using Solidworks and Rhinocerossoftware. A commercial tool called Rhinoceros is used for 3D graphics and computer-aided design (CAD). Software for CA engineering and CAD that models solids is called SolidWorks.

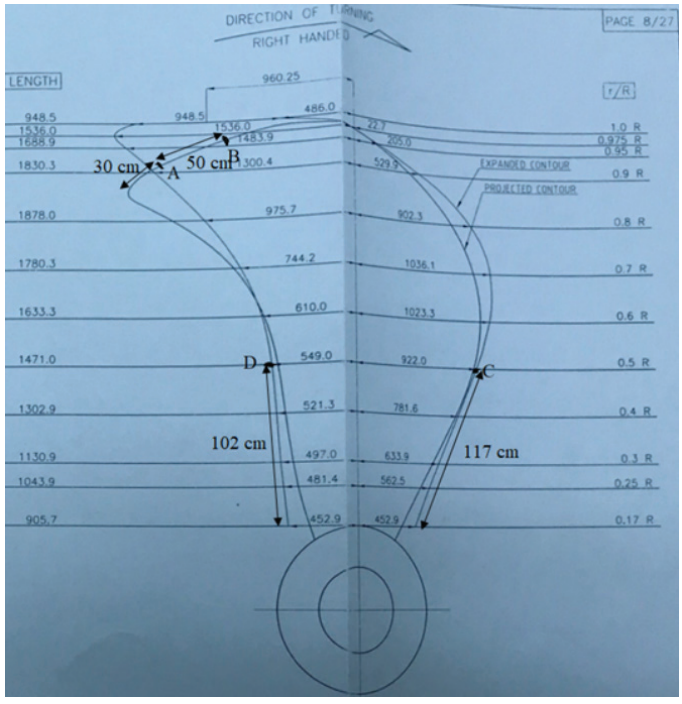

Figure 4. *Propeller blade measurement [20]*

Table 1. *Propeller specifications*

Technical Specifications of the Propeller	
Diameter	D=6.200 m
Pitch at 0.7 R	$P_{0.7}$=4.1362 m
Pitch ratio at 0.7 R	$P_{0.7}$/D= 0.6671
Mean pitch	P_{MEAN}=3.9370 m
Number of blades	Z=4 EA
Expanded area	A_e=15.548 m^2
Expanded area ratio	A_e/A_o= 0.515
Boss ratio	D_{hub}/D=15.548 m^2
Rake	RK=0.0 Deg
Skew	SK=23.856 Deg
Turning direction	Right Handed (Looking from stern)
Material	Ni-Al-Br (CU3)
Section	KH 40
Propeller weight	abt. 17.590 kg
M.O.I in water	abt. 394.340 kg cm s^2
St/Point	454.9 KN
Push up 0 °C	11.98 mm
Push up 35 °C	10.10 mm
Type of ship	Bulk Carrier, Panamax, 80370 dwt
Produced by	Silla Metal Co., Ltd. Drawing No: 09-P-22
Production date	14.05.2010
Approved by	Lloyd's Register (LR BUS1002132)

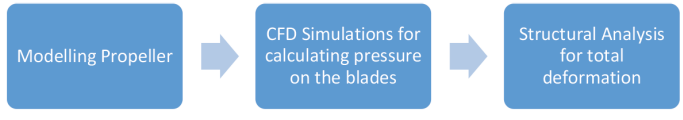

Figure 5. *Operation steps of the computations*

The continuity equation is given by equation (1). The momentum equations are obtained from Equations (2) and (3). If there is a connection between the strain rate and the stress tensor, τ.

A stationary frame can be used to depict the instantaneous equations for mass, momentum, and energy conservation (ANSYS CFX-Solver Theory Guide, November 2009, s.18). The symbols are shown in Table 2.

Engineers simulate interactions in every branch of physics, including vibration, fluid dynamics, and structural analysis, using the general-purpose software Ansys. The unstable Navier-Stokes equations in their conservation form are the set of equations that ANSYS CFX has solved. A chart of the computation operation steps is shown in Figure 5.

$$\frac{\partial \rho}{\partial t} + \nabla \cdot (\rho U) = 0 \quad (1)$$

$$\frac{\partial (\rho U)}{\partial t} + \nabla \cdot (\rho U \otimes U) = -\nabla p + \nabla \cdot \tau + S_M \quad (2)$$

$$\tau = \mu \left(\nabla U + (\nabla U)^T - \frac{2}{3} \delta \nabla \cdot U \right) \quad (3)$$

The total energy equation is written as Equations (4) and (5). where the static enthalpy, h (T,p), is related to the total enthalpy, h_{tot}. The term $\nabla \cdot (U \cdot \tau)$ stands for work caused by viscous strains and is referred to as the viscous work term. The term $U \cdot S_M$, which is currently underutilized, denotes work resulting from external momentum sources.

$$\frac{\partial (\rho h_{tot})}{\partial t} - \frac{\partial p}{\partial t} + \nabla \cdot \left(\rho U h_{tot} \right) = \nabla \cdot (\lambda \nabla T) + \nabla \cdot (U \cdot \tau) + U \cdot S_M + S_E \quad (4)$$

$$h_{tot} = h + \frac{1}{2} U^2 \quad (5)$$

4. Propeller Modeling and Simulation Studies

Three-dimensional modeling of the propeller was performed in accordance with the data from the offset table and propeller sketch [19]. A 3D model of a propeller covered with a frozen shroud was imported into Ansys. The seawater had a depth of 12 m at the time of the incident. As a result, the surrounding environment is defined as a limited zone with a depth of 12 m and a length of 10 m, and the shroud is placed close to the boundary. The geometry of the propeller and shroud and the confined space scenario are shown in Figures 6a and 6b, respectively.

The frozen shroud and propeller were meshed using the following parameters (Physics Reference: CFD, Solver Preference: CFX, Element Order: Linear, Element Size: 9,8,7 cm). With a maximum of 5 layers and a growth rate of 1.2, the mesh's inflation parameters were changed to produce a smooth transition.

Table 2. *The Symbols*

Symbols	
ρ	Density
U	Vector of velocity
p	Pressure
τ	Shear stress, subgrid scale stress, molecular stress tensor
S_M	Momentum source
μ	Molecular (dynamic) viscosity
T	Temperature
δ	Identity matrix or the Kronecker Delta function
h_{tot}	Specific total enthalpy
λ	Thermal conductivity
S_ε	Energy source
h	Specific enthalpy

The settings for a constrained environment were merged (Physics Reference: CFD, Solver Preference: CFX, Element Order: Linear, Element Size: 50, 40, 30 cm). The limited space/shroud boundary size settings were changed to match the size of the shroud element. The following three meshing combinations were tried in order: 9, 8, 7 cm for the shroud element and 50, 40, 30 cm for the restricted space element. Figure 7 displays the mesh modeling of the propeller and shroud. In addition, Figure 8 shows the meshed constrained environment.

Impermeable walls are those found in limited environments, such as the seabed at the bottom and the ice layer at the top. Since it is believed that a revolving propeller cannot initially shatter the ice layer, the ice layer is a wall. The propeller's far parallel plane is known as the inlet, while its opposite plane is known as the outlet. The remaining planes fall within the category of openings. The CFD model of the propeller is shown in Figure 9. The propeller speed is adjustable to three distinct values: 55, 65, and 75 rpm. Seawater having a density of 1 t/m^3 is defined as a flowing substance. The root mean square (RMS), 0.0001, is used as the convergence criterion for the residual target value. Iterations are limited to 800.

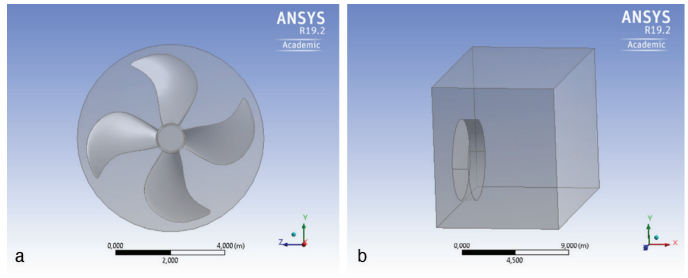

Figure 6. *a) Geometry of the propeller and shroud. b) The confined space scenario*

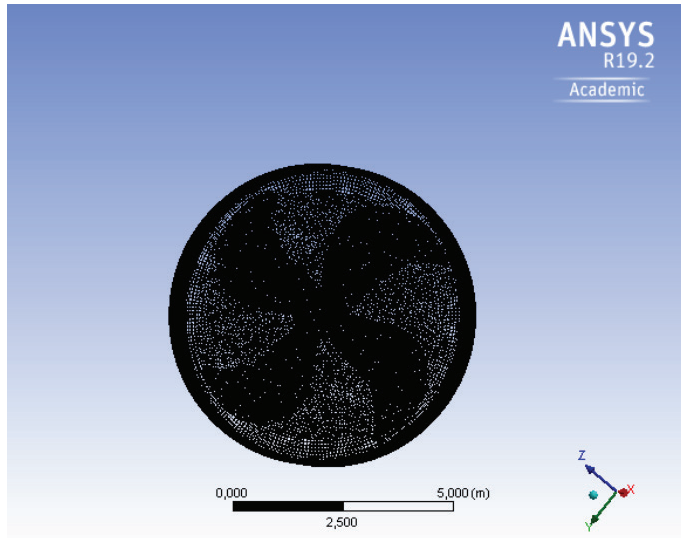

Figure 7. *Meshed modeling of the propeller and shroud*

The CFD solver finished in an auto period of 0.0146912 s, or approximately 9.08 s, at the 618th iteration. ANSYS (2019) claims that while CFX-Solver iteratively approaches the solution, it under-reaches the equations for steady-state scenarios. Using shorter timeframes and under-relaxing limits the amount that the variables vary between iterations. Pressure values were obtained using the CFX Solver (suction side view) at 65 rpm and a 9 cm mesh element size, as shown in Figure 10. Pressure values were obtained using the CFX Solver and a mesh element size of 9 cm for the pressure side view, as shown in Figure 11. Specifications for the propeller alloy material (Cu 3) according to the load register material requirements.

Then, to observe the deformations, the propeller was meshed with elements that were 1 cm smaller than the fixed propeller. Propeller blades that are bent beyond the point of permanent deformation will lose their flexibility due to Push Up, which is 11.98 mm at 0 °C. The pressure values from the CFX Solver were then applied to the propeller in the static structural module. The results of pressure applications of 200,000, 250,000, 300,000, and 350,000 Pascal to normal propeller surfaces were calculated as 1.8207, 2.2758, 2.7310, and 3.1862 cm total deformation, respectively.

Figure 12 illustrates the resulting static structural deformation at 8 cm mesh element size. The blade tip exhibited a maximum deformation of approximately 2.7 cm, as shown in Figure 12.

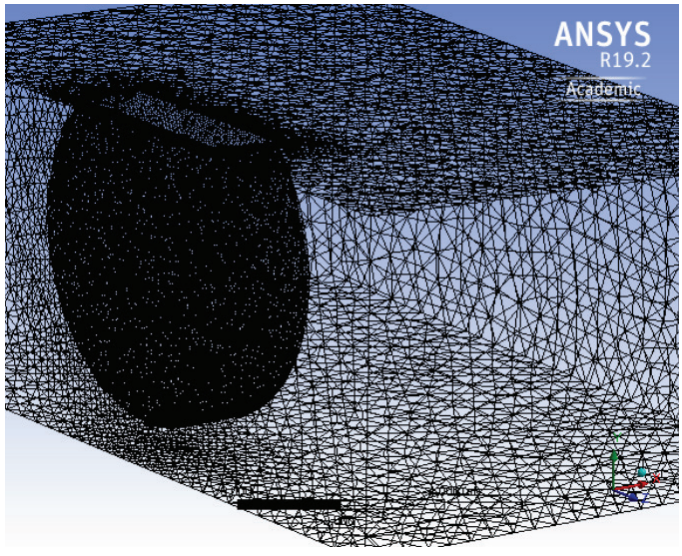

Figure 8. *Meshed confined environment*

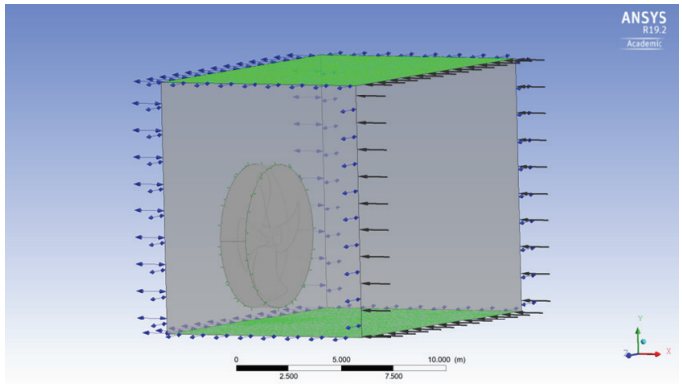

Figure 9. *Walls (green) and openings (gray) in a confined space*

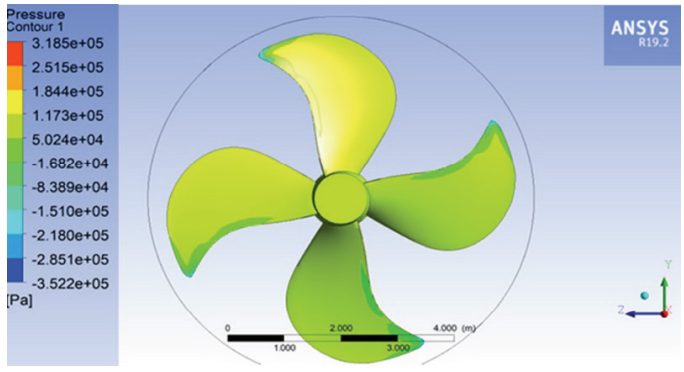

Figure 10. *Pressure values were obtained using the CFX Solver (suction side view) at 65 rpm and a 9 cm mesh element size*

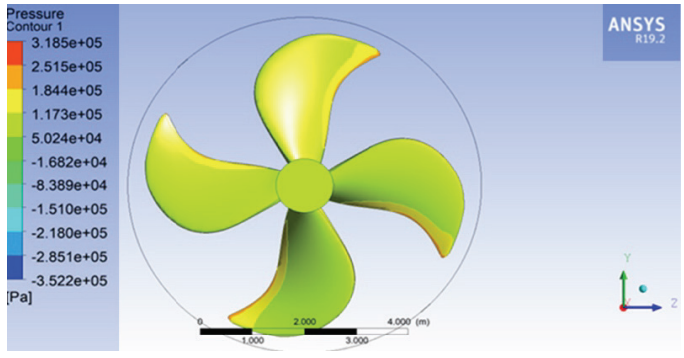

Figure 11*. Pressure values were obtained using the CFX Solver with a mesh element size of 9 cm for the pressure side view*

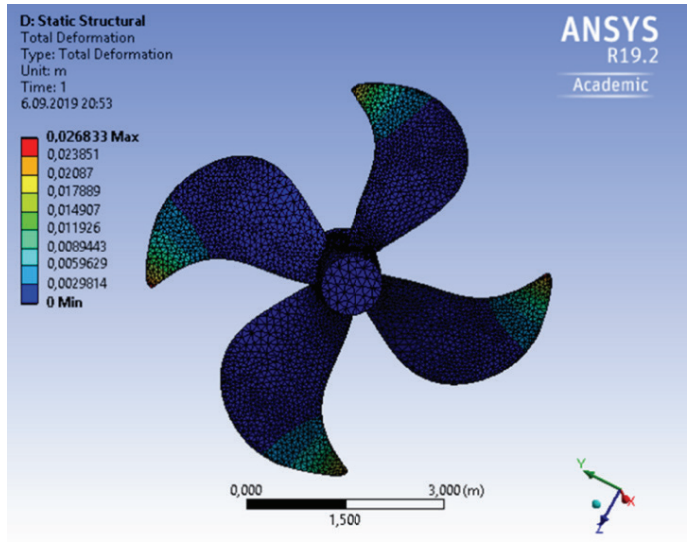

Figure 12*. At 8 cm mesh element size, there is a resultant static structural deformation*

The highest deformation, however, in a static structural module with a 1 cm mesh element size was 2.4704 cm; nonetheless, the black mesh in Figure 12 made it difficult to distinguish the colors of the deformation. Consequently, 8 cm mesh elements were chosen. The difference in mesh element size between 1 cm and 8 cm in the static structural module was only 2.13 mm. The diver's final report stated that the highest measured distortion was around 12 cm. Variations may be attributed to longer exposure periods or different exposure phases to the ice load. It takes less force to bend the blade tip farther once it has been permanently bent.

At various revolutions, the CFX pressure and deformation are produced, as given in Table 3. The study was undertaken to determine the CFX pressure in open water under towage conditions with a propeller turning astern at 65 rpm and the ship's speed at 0 knot. Near the tip, there was just one spot point with a pressure range of 152600 to 218300 Pa. 86920 to 152600 Pa was the pressure range between the nearest line and the trailing edge's tip (the leading edge in astern motion) was 86920 to 152600 Pa. The remaining propeller blades experienced pressures lower than 86920. It can be shown that propellers are typically designed for forward motion when equivalent forward and astern speeds are considered at the same rotation. Therefore, the towage pressure result from the CFX Solver was considered to be normal.

5. Conclusions and Recommendations

This study investigated a marine incident that resulted in a bent propeller blade tip. A vessel vibrated when its tips bent, directing pressurized propeller water toward the aft of the hull. Furthermore, rising exhaust temperatures and increased fuel consumption of the main engine were observed, and the engine's revolution could not be adjusted to match the ship's entire rotation. For normal maintenance of the main engine, 2% of the propeller tips were removed. The tips of the propeller blades were then correctly fixed by welding at the right time and place for propeller condition alignment, which required significant financial and labor investment.

This study aimed to demonstrate that, in addition to the ice contact load assumptions, the subject incident's propeller blade tips bent due to the ice layer's restricted space impact. This study only examined fixed-pitch, right-handed, four-bladed, low-skewed copper alloy (Cu3) propellers, despite the wide variety of propeller types. The primary emphasis of this study was the propeller's astern motion in a constrained environment.

A 12-m-deep enclosed enclosure for the surrounding environment was created by Ansyssliding mesh inserted in a 3D propeller model with a surrounding frozen shroud. The LR material requirements were followed in defining the propeller alloy material (Cu3) parameters.

The following three meshing combinations were conducted in order: 9, 8, and 7 cm for the propeller and frozen shroud element, and 50, 40, and 30 cm for the element in the constrained environment.

The top plane (the ice layer) and bottom plane (the seafloor) of the confined environment are defined by the impermeable wall. The ice coating is believed to function as a wall because the propeller revolves and cannot initially break through it while moving. The opposite plane is designated as the outlet, and the plane far parallel to the propeller is the inlet. The remaining planes are designated as openings. Three distinct propeller rotation values were set: 55, 65, and 75 rpm.

For the residual target value, the convergence criterion was set at 0.0001 RMS. Maximum iteration set to 800. Pressure values from the CFX Solver were then applied to the propeller in the static structural module.

According to the propeller manufacturer's statement, the push-up measures 11.98 mm at 0 °C. This claimed that the propeller blade will become less flexible and undergo irreversible deformation if it is bent by more than 11.98 mm at 0 °C.

The location of the bent at the tip and the blade tip bent area percentage ratio 2% are consistent with the Ansys results. The propeller's rotation can be used to explain the deformation of the three blades. While rotating, the propeller is subjected to high pressure; however, with the Ansys program, the propeller only experiences pressure when it is fixed. The maximum deformation in Ansys was 2.7-3.5 cm, whereas in the incident, it was 12 cm. Longer exposure times or sequential phases in the exposure of the ice load can account for this difference. More deformation can be achieved with less force once the blade tip is permanently bent.

Table 3. *At various revolutions, the CFX pressure and deformation are calculated*

Revolution (rpm)	55			65			75		
Mesh element size (cm)	7	8	9	7	8	9	7	8	9
Maximum pressure (Pascal)	2.603e+05	2.650e+05	2.578e+05	3.234e+05	3.300e+05	3.185e+05	3.980e+05	4.067e+05	3.906e+05
Total deformation (cm)	1.8660	1.8262	1.7842	2.6069	2.5517	2.4704	3.4703	3.3922	3.2825

If the ice layer is sufficiently thick and its suction side is not broken at the start of the vessel's power-driven motion, this leads to an impermeable wall effect that generates pressure and bends the propeller blade until the ice layer is broken.

It must be ensured that a tug or icebreaker breaks the propeller suction side of the ice layer to prevent bent blades. Even a small trail will be sufficient to release the pressure. When the ship accelerates, its displacement (mass) will be sufficient to break the ice.

In addition, placing high-pressure sensors near the propeller at the bottom of the hull can be advised. These sensors will turn off the main engine when the high-pressure level is set. The Polar Code can analyze ice-class propellers using this form of enclosed space modeling if it receives approval from IACS. Nonetheless, further materials science research can be conducted to investigate the use of stronger, more resilient materials because the tips and edges of a blade are by nature their thinnest parts.

Acknowledgments

The authors would like to thank Dr. Metin Aytekin Demir who supported them with his kind assistance in this study.

Authorship Contributions

Concept design: M. Ertogan, Data Collection or Processing: A. Bozkurt, Analysis or Interpretation: M. Ertogan, and A. Bozkurt, Literature Review: A. Bozkurt, Writing, Reviewing and Editing: M. Ertogan, and A. Bozkurt.

Funding: The authors received no financial support for the research, authorship, and/or publication of this article.

References

[1] D. Walker, N. Bose, H. Yamaguchi, and S. J. Jones, "Hydrodynamic loads on ice-class propellers during propeller-ice interaction." *Journal of Marine Science and Technology,* vol. 2, pp. 12-20, Mar 1997.

[2] D. L. N. Walker, *The influence of blockage and cavitation on the hydrodynamic performance of ice class propellers in blocked flow*. Memorial University of Newfoundland, 1996.

[3] H. Soininen, *A propeller-ice contact model.* VTT Technical Research Centre of Finland, VTT Publications 343, 1998.

[4] J. Wang, et al. "Ice loads acting on a model podded propeller blade." *Journal of Offshore Mechanics and Arctic Engineering,* vol. 129, pp. 236-244, Aug 2007.

[5] S. K. Lee, "Engineering practice on ice propeller strength assessment based on IACS polar ice rule-URI3." *ABS Technical Papers,* 2007.

[6] P. Liu, N. Bose, and B. Veith, "Evaluation, design and optimization for strength and integrity of polar class propellers" *Elsevier Cold Regions Science and Technology,* vol. 113, pp. 31-39, May 2015.

[7] A. Kinnunen, V. Lamsa, P. Koskinen, M. Jussila, and T. Turunen, "Marine propeller-ice interaction simulation and blade flexibility effect on contact load" in *Proceedings of the 23rd International Conference on Port and Ocean Engineering under Arctic Conditions, Trondheim, Norway,* June 14-18, 2015.

[8] L. Y. Ye, and C. Wang, "Propeller-ice contact modeling with peridynamics." *Ocean Engineering,* vol. 139, pp. 54-64, Jul 2017.

[9] W. Chao, S. Sheng-Xia, C. Xin, and Y. Li-yu, "Numerical simulation of hydrodynamic performance of ice class propeller in blocked flow–using overlapping grids method." *Ocean Engineering,* vol. 141 pp. 418-426, Sep 2017.

[10] C. Wang, X. Li, X. Chang, and W. P. Xiong, "Numerical simulation of propeller exciting force induced by milling-shape ice." *International Journal of Naval Architecture and Ocean Engineering,* vol. 11, pp. 294-306, Jan 2019.

[11] L. Y. Ye, C. Y. Guo, C. Wang, C. H. Wang, and X. Chang, "Strength assessment method of ice-class propeller under the design ice load condition." *International Journal of Naval Architecture and Ocean Engineering* vol. 11, pp. 542-552, Jan 2019.

[12] C. Y. Guo, P. Xu, C. Wang, and W. P. Xiong, "Experimental investigation of the effect of ice blockage on propeller hydrodynamic performance." *Hindawi Mathematical Problems in Engineering,* vol. 2019, pp. 1-19.

[13] L. Zhou, S. Zheng, S. Ding, C. Xie, and R. Liu, "Influence of propeller on brah ice loads and pressure fluctuation for a reversing polar ship" *Ocean Engineering*, vol. 280, pp. 114624, 2023.

[14] C. Xie, L. Zhou, S. Ding, R. Liu, and S. Zheng, "Experimental and numerical investigation on self-propulsion performance of polar merchant ship in brash ice channel" *Ocean Engineering*, vol. 269, pp. 113424, Feb 2023.

[15] A. Zambon, L. Moro, A. Kennedy, and D. Oldford, "Torsional vibrations of Polar-Class shaftlines: Correlating ice–propeller interaction torque to sea ice thickness*" Ocean Engineering*, vol. 267, pp. 113250, Jan 2023.

[16] R. Matala, and M. Suominen, "Investigation of vessel resistance in model scale brash ice channels and comparison to full scale tests" *Cold Regions Science and Technology*, vol. 201, pp. 103617, Sep 2022.

[17] F. Li, F. Goerlandt, and P. Kujala, "Numerical simulation of ship performance in level ice: A framework and a model" *Applied Ocean Research*, vol. 102, pp. 102288, Sep 2020.

[18] Y. Xue, R. Liu, Z. Li, and D. Han, "A review for numerical simulation methods of ship–ice interaction" *Ocean Engineering*, vol. 215, pp 107853, Nov 2020.

[19] A. Bozkurt, *Marine Propeller Blade Structure Analysis in Ice Navigation*. ITU Graduate School of Science Engineering and Technology, Maritime Transportation Engineering Program, September 2019.

[20] J. Y. Lee, Sil La Metal Co., Ltd. Propeller drawing, (Drawing No: 09-P-22), September 2010.